UC Riverside
UC Riverside Previously Published Works

Title
Chemical Fate of Particulate Sulfur from Nighttime Oxidation of Thiophene

Permalink
https://escholarship.org/uc/item/0nt234cx

Journal
ACS ES&T Air, 1(12)

ISSN
2837-1402

Authors
Lum, Michael
Chen, Kunpeng
Ries, Bradley
et al.

Publication Date
2024-12-13

DOI
10.1021/acsestair.4c00164

Copyright Information
This work is made available under the terms of a Creative Commons Attribution-NonCommercial-NoDerivatives License, available at https://creativecommons.org/licenses/by-nc-nd/4.0/

Peer reviewed

eScholarship.org Powered by the California Digital Library
University of California

ACS ES&T Air

Open Access
This article is licensed under CC-BY-NC-ND 4.0
pubs.acs.org/estair

Article

Chemical Fate of Particulate Sulfur from Nighttime Oxidation of Thiophene

Published as part of ACS ES&T Air special issue "Wildland Fires: Emissions, Chemistry, Contamination, Climate, and Human Health".

Michael Lum, Kunpeng Chen, Bradley Ries, Linhui Tian, Raphael Mayorga, Yumeng Cui, Nilofar Raeofy, David Cocker, Haofei Zhang, Roya Bahreini,* and Ying-Hsuan Lin*

Cite This: *ACS EST Air* 2024, 1, 1637−1649

Read Online

ACCESS | Metrics & More | Article Recommendations | Supporting Information

ABSTRACT: Sulfur-containing volatile organic compounds emitted during wildfire events, such as dimethyl sulfide, are known to form secondary aerosols containing inorganic sulfate (SO_4^{2-}) and surfactant-like organic compounds; however, little is known about the fate of sulfur in other emitted reduced organosulfur species. This study aimed to determine the sulfurous product distribution resulting from the nighttime oxidation of thiophene as a model system. Ion chromatography (IC) and aerosol mass spectrometry (a mini aerosol mass spectrometer, mAMS) were used to constrain the proportions of sulfurous compounds produced under wildfire-relevant conditions ($[NO_2]/[O_3] = 0.1$). With constraints from IC, results indicated that the sulfurous particle mass consisted of 30.3 ± 6.6% SO_4^{2-}, while mAMS fractionation attributed 24.5 ± 1.6% of total sulfate signal to SO_4^{2-}, 15.4 ± 1.9% to organosulfates, and 60.1 ± 0.9% to sulfonates. Empirical formulas of organosulfur products were identified as C1−C8 organosulfates and sulfonates using complementary mass spectrometry techniques. This study highlights the nighttime oxidation of thiophene and its derivatives as a source of SO_4^{2-} and particulate organosulfur compounds, which have important implications for the atmospheric sulfur budget and aerosol/droplet physical and chemical properties.

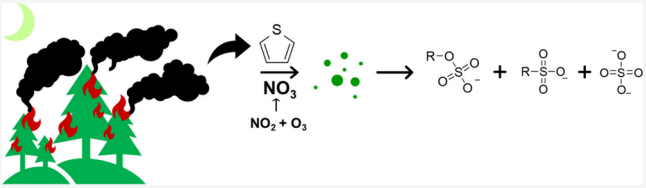

KEYWORDS: *volatile organosulfur, wildfire, biomass burning, nighttime chemistry, sulfate, sulfonate, organosulfate, secondary aerosol*

1. INTRODUCTION

The growing prominence and frequency of wildfires have not only changed the distribution of elements such as sulfur throughout the environment, but also the potential chemical pathways available to pollutants within it. Large-scale wildfires are causing disruption to the normative sulfur distribution and volatilizing sulfur present in biomass.[1] Although sulfur is volatilized more dominantly as sulfur dioxide (SO_2) during biomass burning with emission factors up to ∼0.68 g SO_2/kg burned,[2] wildfires have been reported to emit reduced organosulfur species such as dimethyl sulfide (DMS),[3−5] thiophene, and methyl thiophene in large quantities.[6,7] The fate of sulfur during the atmospheric oxidation of these precursors has yet to be fully constrained under nighttime conditions.[4,5,8] Rapid volatilization and oxidation of these species may result in production of secondary aerosols (SA) containing sulfurous products of differing environmental impacts, structures, and sulfur oxidation state−namely, inorganic sulfate (SO_4^{2-}), organosulfates (OS), and sulfonates.[9−12] Hence, predicting the fate and distribution of sulfur-containing products formed during volatile organic compound (VOC) oxidation remains vital to understanding their impacts on atmospheric chemical composition and physical characteristics.

Under daytime conditions, hydroxyl (OH) radicals are well established as predominant oxidants in oxidation reactions, with photolysis of ozone (O_3) serving as a key step in their formation. While many theoretical, laboratory and field studies have examined the oxidation behavior of thiophene under daytime conditions,[8,13−21] the nighttime chemistry of thiophene oxidation is largely unknown. Only a few studies have investigated thiophene reactivity against nitrate (NO_3) radicals and have primarily focused on the kinetics and initiation steps of the mechanism, with very little discussion of compounds produced through multigeneration oxidation.[22−26] Ozonolysis of thiophene has also not had its mechanism investigated for conclusive evidence of proposed products. The mechanism for gaseous ozonolysis of olefins proceeds through the formation

Received: July 17, 2024
Revised: November 20, 2024
Accepted: November 21, 2024
Published: November 27, 2024

ACS Publications

© 2024 The Authors. Published by American Chemical Society

of a primary ozonide and rapid decomposition into Criegee intermediates and a pair of carbonyl products.[27] However, Kaduk et al.[21] propose that O_3 could form a primary ozonide with the S and α-carbon. Nighttime chemistry is a complex mixture of oxidants, suggesting the oxidation of thiophene may be a competition between NO_3, OH, O_3, hydroperoxyl radical (HO_2), and intermediate oxidation species such as Criegee biradicals. This study aims to investigate the production of oxidized sulfur under these complex dark conditions, which represents nighttime oxidation mechanisms possible in a biomass burning plume.

Oxidized forms of sulfur have been initially explored as products of DMS oxidation and SO_2 multiphase reactions, as well as for their impact on particle physical and chemical properties;[4,28−32] however, the fate of other volatile organosulfur compounds, such as thiophene, and the distribution of sulfurous products in secondary aerosols have yet to be thoroughly characterized. With an emission factor of $(4.6 \pm 1.2) \times 10^{-3}$ g thiophene/kg biomass burned from common west coast vegetation such as the Ponderosa Pine,[6] thiophene and other heterocyclic aromatic wildfire pollutants may be increasingly concentrated in and downwind of burn areas, and thus exposure estimations and gas-aerosol chemical conversion mechanisms may not currently account for products in these environments. Similarly, thiophene emission was observed from wildfires during the recent 2016 FIREX campaign with magnitudes similar to DMS emissions at an emission rate of 0.014 g/kg fuel burned,[33] or 0.057 ppb thiophene/ppm carbon monoxide (CO) emitted. Since a maximum of 600 ppm has been reported for CO concentrations near sources of wildfire plumes,[34] thiophene concentrations near sources are expected to be ∼34 ppb. This has called into question whether the fate of the sulfur atom under wildfire conditions is being properly accounted for under current atmospheric processing predictions. Recent discoveries by Decker et al.[35] have revealed that the high VOC reactivity in biomass burning plumes can cause the rate of reactions with NO_3 to exceed both the photolysis rate and nitric oxide (NO) reaction, thereby allowing NO_3 chemistry to dominate during typical daylight hours. This study suggests that oxidation by NO_3 mechanisms resulting from reactions between nitrogen dioxide (NO_2) and O_3 may play a more widespread and crucial role than previously thought when considering sulfur atmospheric distribution.

The objective of this study was to constrain the distributions of sulfonates, OS, and SO_4^{2-} produced by the NO_3 oxidation of thiophene as a model system relevant to biomass burning. As aromatic VOCs, thiophene and its derivatives represent an understudied yet critical component during wildfire events that may potentially impact the ecosystem-wide sulfur cycling.[2,5,6] A unique combination of online and offline instrumentation was used to quantify and identify major sulfur-containing products at $[NO_2]/[O_3]$ ratios observed within wildfire plumes. We hypothesize that reduced volatile organosulfur pollutants are a currently unaccounted source of SO_4^{2-}, OS, and sulfonate compounds in the atmosphere and that distributions of these products will be impacted by NO_3 as an oxidant. Ion chromatography (IC) and mass spectrometry (a mini-Aerosol Mass Spectrometer (mAMS)) were used to constrain the distribution of sulfur within SO_4^{2-}, sulfonates, and OS compounds. Through utilization of complementary MS techniques coupled to chromatographic separation, empirical formulas and functional group information on several major sulfur-containing products were obtained. Results of this study will further improve understanding of the atmospheric sulfur budget and distribution of sulfurous compounds and thus capability of models to predict particle composition, acidity, and surface tension.

2. METHODS

2.1. Chamber Experiments for Aerosol Generation. Experiments were carried out in a 10 m^3 fluorinated ethylene propylene (FEP) film indoor chamber under conditions typical for nighttime oxidation under low relative humidity (<20%). The temperatures were maintained constant throughout oxidation experiments (22 ± 4 °C). Further details on experimental set up can be found in SI Text S1−S3 or within our prior publications.[36−41] This study focused on investigating oxidation products observed under nighttime oxidation conditions attributed to NO_3 produced by the reaction of NO_2 and O_3. Although the ratio and concentration of NO_3 precursors vary greatly with distance from the source, the focus of this study was not to identify the effect of NO_3 concentration on thiophene products. An assumption was made that $[NO_2]/[O_3] = 0.1$ was representative of a somewhat processed wildfire plume observed by Singh et al.[42] Furthermore, we will not investigate the fate or reaction of peroxy radicals, which may be sensitive to this ratio. Absolute concentrations of oxidant precursors for each experiment used to achieve the biomass burning condition ratio observed by Singh et al.[42] are shown in Table S1.

Thiophene reagent (Alfa Aesar, 99%) was introduced in the chamber using a small glass jar wrapped with a heating coil to ensure a consistent elevated temperature (>90 °C) for complete volatilization of thiophene. Thiophene was injected into the heated glass jar and flushed into the FEP chamber using 15 LPM zero air as a carrier gas. A target mixing ratio of 200 ppbv thiophene was selected for this set of experiments, and oxidation was allowed to proceed for 3 h. Previous model predictions conducted by Mayorga et al.[36] showed a theoretical NO_3 concentration of ∼8 ppb under experimental NO_2/O_3 conditions before VOC introduction. The lifetime of thiophene against NO_3 and O_3 were determined based on the rate constants reported by Atkinson et al.[13,26] The lifetime of thiophene against NO_3 oxidation was calculated to be ∼2.6 min ($k = 3.2 \times 10^{-14}$ cm^3 $molecule^{-1}$ s^{-1}, calculated for 8 ppbv NO_3), while the lifetime of thiophene against O_3 was calculated to be >5.2 days ($k < 6 \times 10^{-20}$ cm^3 $molecule^{-1}$ s^{-1}, calculated for 1500 ppbv O_3). While the reaction rate constant of thiophene with O_3 is several orders of magnitude slower than the reaction with NO_3,[13,26] the concentration of O_3 is several orders of magnitude higher than NO_3 under $[NO_2]/[O_3] = 0.1$. This implies, while initially thiophene reacts with NO_3, subsequent oxidation of later generation products is likely a competition between O_3 and NO_3, as well as OH radicals produced by ozonolysis of early generation products or reactions between NO_3 and HO_2. The competition between O_3, NO_3 radicals, OH radicals, and Criegee intermediates may change the product distribution or observed product identity during the SOA formation process if an individual oxidant favors the formation of SO_4^{2-}, OS, or sulfonate products. Additional oxidative species formed throughout the initial phases of the experiment, such as OH radicals formed through ozonolysis or NO_3 reactions with HO_2, may play a role in later phases of oxidation. Other oxidizing species likely present and able to participate in reactions include HO_2, RO_2, and RO radicals. All of these

https://doi.org/10.1021/acsestair.4c00164
ACS EST Air 2024, 1, 1637−1649

species are formed through expected reactions under nighttime conditions for VOC oxidation and thus should not be discounted or excluded. Within this study we were not able to determine the branching ratio of competing oxidation pathways and greater mechanistic detail; however, this should be further investigated in future studies. To distinguish the major products and relative product distributions resulting from the NO_3 oxidation pathways against ozonolysis, control experiments were performed with O_3 as the only oxidant. Next, an additional O_3-only experiment was performed to test the impact of OH radicals during these O_3 experiments using 1-butanol as an OH scavenger.[43] These experiments were performed identically to O_3-only control experiments; however, 200 ppm of 1-butanol (Fisher Chemical, > 99%) was injected prior to thiophene VOC injection. Separate thiophene oxidation experiments with nitric anhydride (N_2O_5) as the precursor for NO_3 formation were also conducted as an O_3-free control. As is obvious in Figure S2 the N_2O_5 present in O_3-free controls is much higher than in NO_2/O_3 experiments. Figure S3 shows the modeled concentration of NO_3 under NO_2/O_3 conditions. Since N_2O_5 breaks down into NO_2 and NO_3, Table S1 suggests that the NO_3 concentrations under N_2O_5 conditions were much higher than under NO_2/O_3 conditions. The experimental conditions for N_2O_5 and O_3-only control experiments are depicted in Figure S4.

The SA formation progress during chamber experiments was monitored using a Scanning Electrical Mobility Spectrometer (SEMS, Brechtel Mfg.) to determine the particle size distribution and volume concentrations in real time. The SEMS was set to scan from 10 to 800 nm with 120 bins and a total scan time of 120 s. Aerosol bulk composition was monitored online by a mini aerosol mass spectrometer equipped with a compact time-of-flight (C-ToF) mass spectrometer (mAMS, Aerodyne Research Inc.). Integrated volume concentration was converted to mass concentration using aerosol effective density (discussed below). Filter mass loading was calculated by multiplying the volume concentration measured by SEMS by the density estimated by the mAMS, the collection flow rate, and the duration of the filter collection period. Experiments were performed in triplicate (n = 3) for each condition to ensure reproducibility of the results.

2.2. Quantitative Analysis of SA Bulk Composition. As mentioned before, chemical composition and sulfur fate were investigated through a combination of online and offline instrumentation. The mAMS provided concentrations of organic, sulfate, and nitrate aerosols. Particle effective density was calculated through a comparison of the mode of mAMS mass distributions and the mode of SEMS volume distributions.[44,45] Assuming spherical particles and unit density (ρ_0) of 1 g/cm^3, aerosol effective density was calculated using eq 1 that relates vacuum aerodynamic diameter mode (d_{va}) measured by the mAMS to mobility diameter mode (d_m) measured by the SEMS.[44,45]

$$\rho_{eff} = \frac{d_{va}}{d_m}\rho_0 \tag{1}$$

To determine the concentration of SO_4^{2-}, filters were extracted into 7 mL of Milli-Q water, diluted by 1:1 sample to Milli-Q water, and analyzed by a Dionex Aquion IC system (Thermo Fisher Scientific). The IC system was equipped with a Dionex IonPac AS14 (4 × 250 mm, Thermo Scientific) column and operated using a 0.1 M carbonate/bicarbonate isocratic mobile phase elution. To ensure proper separation and peak sensitivity, an analysis time of 21 min per 5 mL sample was selected. A 7-point calibration curve covering the range of 0.1 ppm-50 ppm of SO_4^{2-} was obtained prior to analyzing each set of samples.

Due to the nature of the mAMS utilizing electron impact (EI) hard ionization, the total sulfate fraction accounts for all species that fragment into SO^+ (m/z 48), SO_2^+ (m/z 64), SO_3^+ (m/z 80), HSO_3^+ (m/z 81), and $H_2SO_4^+$ (m/z 98). Thus, SO_4^{2-}, OS, and sulfonates all contribute to the fraction of sulfate observed by the mAMS. This total sulfate concentration was estimated from the volume concentrations measured by SEMS, multiplied by the calculated effective density and sulfate fraction (f_{SO_4}) of the aerosols as provided by the mAMS, while the SO_4^{2-} mass concentration was determined by IC. By subtracting the mass concentration of SO_4^{2-} from the total sulfate mass concentration observed by the mAMS, the mass concentration of sulfate fragments arising from organic molecules (e.g., OS or sulfonates) was calculated. The percentages of total particle sulfur in the inorganic and organic forms formed by NO_3 oxidation in NO_2/O_3 experiments were contrasted with the control experiments (i.e., ozonolysis) to demonstrate the dependence of product distribution on NO_3 oxidation. These results were compared to a novel mAMS fractionation method based on approaches taken by Chen et al.[46] to determine the relative proportion of SO_4^{2-}, OS, and sulfonate products that contribute to the total sulfate fragments measured by mAMS.

Despite the extensive fragmentation that occurs during mAMS measurements, fragmentation patterns may be used to approximate the fractions of various sulfur-containing species in mAMS data using multiple sulfur-containing standards as references.[46] In the current work, seven standards (ethyl sulfate, ≥98% Sigma-Aldrich; potassium phenyl sulfate, ≥98% Sigma-Aldrich; potassium nitrophenyl sulfate, ≥98% Sigma-Aldrich; sodium octyl sulfate, 99%, Alfa Aesar; propanesulfonate, 99% Sigma-Aldrich; benzenesulfonate, 97% Sigma-Aldrich; sulfuric acid, 95−98% Hach) were nebulized into the mAMS, and signal intensities of the main sulfur-containing fragments (SO^+ (m/z 48), SO_2^+ (m/z 64), SO_3^+ (m/z 80), HSO_3^+ (m/z 81), $H_2SO_4^+$ (m/z 98)) were recorded at multiple aerosol concentrations. The signal ratios of m/z 64, 80, 81, and 98 to m/z 48 were calculated to highlight the differences in fragmentation patterns of the three classes of compounds (sulfonate, OS, or SO_4^{2-}). Table S2 shows the results of fragmentation of each standard run, while Table S3 shows the average and standard deviations of the fragment ratios calculated for the sulfur compound classes. Based on these results, it was determined that these compounds show a more unique fragmentation pattern at SO_3^+ and HSO_3^+ relative to SO^+ (i.e., m/z 80/48 and m/z 81/48). Assuming that the sulfate signal in the experiments is a linear combination of signals from SO_4^{2-}, OS, and sulfonate, the average ratios of m/z 80/48 and m/z 81/48 from the standard compounds were compiled in a system of equations shown below and solved for the fraction of inorganic sulfate ($f_{SO_4 i}$), organic sulfate (f_{OS}), and sulfonates (f_{sulfon}).

$$\left(\frac{80}{48}\right)_{observed} = 0.541(f_{SO_4 i}) + 0.062(f_{sulfon}) + 0.427(f_{OS}) \tag{2}$$

https://doi.org/10.1021/acsestair.4c00164
ACS EST Air 2024, 1, 1637−1649

$$\left(\frac{81}{48}\right)_{\text{observed}} = 0.316(f_{SO_4 i}) + 0.135(f_{\text{sulfon}}) + 0.008(f_{OS}) \quad (3)$$

$$1 = (f_{SO_4 i}) + (f_{\text{sulfon}}) + (f_{OS}) \quad (4)$$

The observed ratios of 80/48 and 81/48 from the end of each experiment (corresponding to the start of filter collection) were used in eqs 2 and 3, and the system of equations was solved to determine the fractional contribution of each sulfur-containing product type to the sulfate signal observed by the mAMS.

A two-way ANOVA test was performed to determine the statistical significance of the differences in product distributions observed with the different oxidants. Šidák and Tukey multiple comparison *posthoc* analyses were performed using GraphPad Prism 9 to determine statistical significance of attributed fractions between experimental oxidation conditions. A resulting p value of $p < 0.05$ was considered statistically significant.

2.3. Qualitative Analysis of SA Molecular Composition. Multiple filter samples were collected from each experiment for offline IC, LC/MS, and a Filter Inlet for Gases and AEROsols coupled to a time-of-flight-chemical ionization mass spectrometer (FIGAERO-ToF CIMS) analyses to quantify SO_4^{2-} and identify sulfur-containing organic products. A more detailed procedure for filter collection is provided in SI, Text S3. One set of filter samples was analyzed with the FIGAERO-ToF CIMS set up in offline desorption mode. The instrument was operated using iodide (I^-) as the reagent ion. The thermal desorption temperature profile used consisted of a ramping phase from 30 to 200 °C over a 15 min interval, an isothermal soaking phase held for 25 min, and then a 5 min cooling phase. Data were interpreted using the Tofware v3.2.5 package through Igor Pro (WaveMetrics).

Samples were sonicated for 50 min to extract SA into MeOH and concentrated into a 150 μL solution for LC/MS analyses. Additional tests were carried out to compare the sonication extraction procedures to vortex extraction procedures to ensure sonication did not affect quantification or identification of species during offline analysis. The EIC and mass spectra of the standard undergone through sonication and vortex extraction are shown in Figure S4, and the IC findings are reported in Text S4. Samples were first analyzed using a liquid chromatography triple quadrupole mass spectrometer (LC/QQQ-MS) with precursor ion scan to identify SA constitutes that fragment into $SO_4^{-\bullet}$, HSO_4^-, $SO_3^{-\bullet}$, and HSO_3^-,[47] enabling a subsequent targeted search for their parent compounds using the high-resolution tandem mass spectrometry methods (i.e., LC/Q-ToF-MS). The precursor ion scan was performed using an Agilent Technologies 1290 Infinity II LC system and 6470 triple quadrupole MS equipped with an electrospray ionization (ESI) ion source and operated in negative ion mode. A 2.1 mm × 100 mm UPLC BEH Amide Column (Waters ACQUITY) with a 1.7 μm particle size was used for chromatographic separation.

High-resolution MS data was obtained by analyzing the same solution using LC/Q-ToF-MS. Analysis was performed on an Agilent 6545 LC-ESI-Q-ToF-MS with an Agilent Poroshell 120 EC-C18 column (3.0 × 50 mm, 2.7 μm particle size). For structural elucidation, the parameters and column used for LC/Q-ToF-MS were replicated for tandem MS analysis with a collision energy of 30 eV. This enabled the confirmation of the OS and sulfonate candidates based on the accurate mass fittings of the measured mass spectral peaks.

3. RESULTS AND DISCUSSION

The real-time concentrations of NO_2 and O_3 during SA formation in typical chamber experiments are shown in Figure 1, labeled according to the experimental step to display

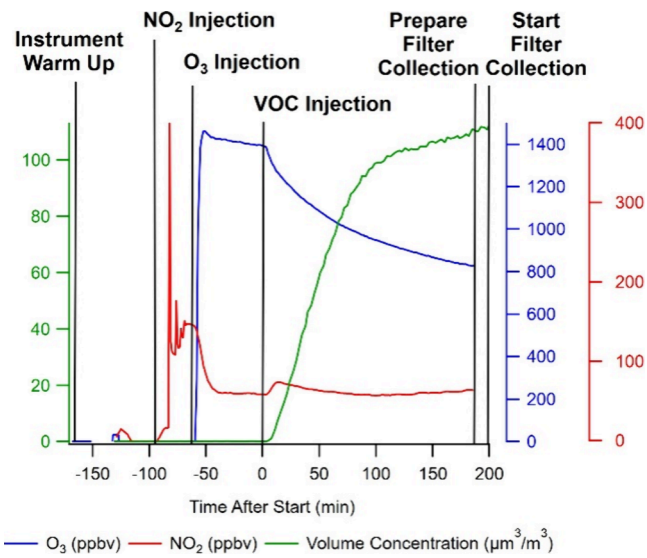

Figure 1. Reaction progress during the NO_2/O_3 experiment, with the gas phase oxidant precursors and VOC concentrations plotted along with the time series of secondary aerosol volume concentrations.

different phases of the reaction. Inspection of the concentration curve for NO_2 shows a drastic decrease upon injection of O_3, indicating the start of NO_3 formation. The stabilization of NO_x concentrations is a result of limitations of the NO_x analyzer reading a combination of NO, NO_2, N_2O_5, and NO_3,, HONO, $RONO_2$, $ClNO_2$, and peroxyacetyl nitrates.[48] This plateau corresponds to the establishment of an equilibrium. The initial drop in NO_x corresponds to the reaction of 2 NO_2 molecules reacting with one O_3 molecule to form N_2O_5. O_3 would then decrease much more rapidly than the NO_2 curve, as the analyzer is still detecting the other reservoirs of NO_2,[48] while the O_3 curve represents the absolute concentration. Figure S1 shows a decrease in N_2O_5 levels, which implies a decreased presence of NO_3 in later stages of the experiment. Oxidation of later-generation products may therefore be a competition between NO_3 and O_3 as oxidants under NO_2/O_3 experimental conditions. Figure S3 depicts the experimental conditions for N_2O_5 and O_3-only control experiments.

Figure 2 depicts the mass fractions of nitrate (broken down into organic and inorganic nitrate), sulfate, and organics as measured by mAMS. Reported numbers were the average of measurements taken over the final 10 min before aerosol filter collection began. Sulfate contributed to 26.6 ± 0.58% of the bulk composition of particles formed. This contrasted with the two other conditions, with the O_3-only control conditions showing a higher fraction of sulfate with an average of 34.2 ± 1.74%. N_2O_5 control conditions showed a sulfate fraction of 11.4 ± 0.69%, which was significantly lower than the other two conditions. This confirmed that SA products observed under the NO_2/O_3 condition could not be attributed solely to either NO_3 or O_3 reactions, while O_3 only and N_2O_5 conditions

https://doi.org/10.1021/acsestair.4c00164
ACS EST Air 2024, 1, 1637−1649

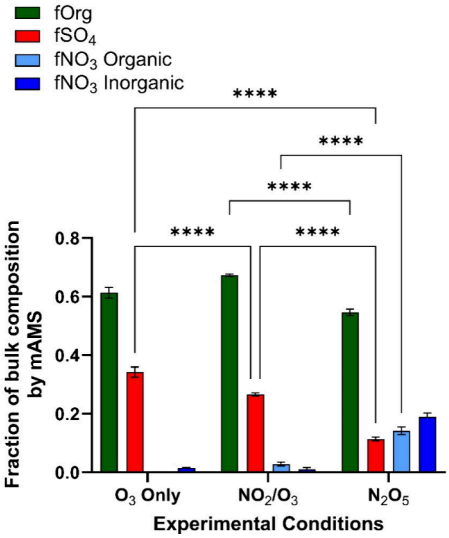

Figure 2. Bulk composition of aerosols as seen by mAMS for each oxidation condition broken down into mass fraction of components containing nitrate (fNO_3), mass fraction of components containing sulfate (f_{SO_4}), and mass fraction of organics (fOrg). The f_{SO_4} signal consists of all fragments of sulfate detected by the mAMS. Nitrate observed under O_3-only conditions was attributed to inorganic nitrate, as signal was too low to accurately determine the fractions of inorganic and organic nitrate. Statistical differences were observed between the fraction of bulk composition associated with sulfate and organic nitrate under all three oxidation conditions. Statistical significance with a p value < 0.0001 was represented as ****.

could be used as controls for chamber experiments since the observed differences between sulfate fractions and organic nitrate fractions under each condition are significant (p < 0.0001), as determined by the Tukey multiple comparisons test. Total nitrate fraction also differed between the three conditions, with N_2O_5 showing a much larger fraction of nitrate (33.1 ± 1.38%), likely due to the uptake of N_2O_5 and subsequent hydrolysis into inorganic nitrate under these experimental conditions. O_3 only showed 1.5 ± 0.02% nitrate, likely due to revolatilization of nitrate-containing components deposited on chamber walls during prior experiments.

The nitrate fraction of products observed under NO_2/O_3 and N_2O_5 conditions was broken down into organic (as organic nitrate or nitroorganic) and inorganic nitrate contributions following procedures outlined in prior studies.[49,50] Organic nitrate/nitroorganic contributed to ∼14.2% and ∼1.0% of aerosol bulk composition in N_2O_5 conditions and NO_2/O_3 conditions, respectively. Organic nitrate is commonly used as a marker of nighttime chemistry, as NO_3 will preferentially add to olefins at the most substituted carbon.[51] Inorganic nitrate in either condition may result from either hydrogen abstraction or uptake of N_2O_5 followed by subsequential hydrolysis under these conditions. Inorganic nitrate is assumed to be either nitric acid or a nitrate salt. The differences in fraction of bulk composition between atmospheric conditions and control experiments show that O_3 may play a more critical role in the oxidation of second- and later-generation products than previously thought.

The formation of SO_2 was monitored using the online ToF-CIMS over the course of the experiment. SO_2 is well-known to oxidize further in both the gas and aqueous phases to form SO_4^{2-}, leading to the potential acidification of droplets and particles.[30,52,53] Gaseous SO_2 has been shown to be oxidized to SO_4^{2-} by stabilized Criegee intermediates (sCIs) in the atmosphere.[54] SCIs are formed through the ozonolysis of olefins.[55,56] The formation of SO_2 over time under the NO_2/O_3 condition is shown in Figure 3. As discussed in Section 3.1

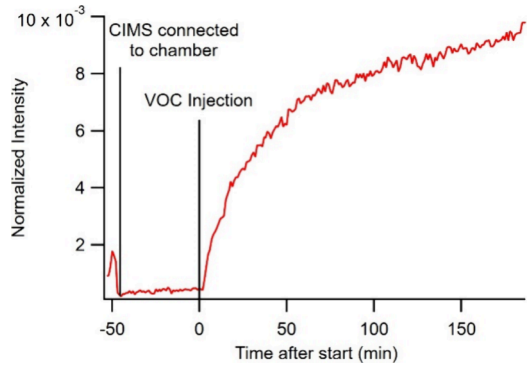

Figure 3. Gaseous SO_2 formation after injection of thiophene (i.e., VOC) under atmospherically relevant nighttime conditions. The signal intensity was normalized to the I^- + $(H_2O)I^-$ signal.

below, the fractions of SO_4^{2-} differed between the two experimental conditions. The formation of SO_2 is a likely pathway for the formation of SO_4^{2-} under nighttime atmospheric conditions. SO_2 emissions from biomass burning have been defined as a primary emitted pollutant with an emission factor ranging from 0.24 to 0.66 g/kg in Boise, Idaho, and Salina, Kansas, during the recent FIREX-AQ campaign,[57] as well as those observed by Andreae et al.[58] within the Amazon basin. As shown by Cabañas et al.,[23] the NO_3 radical will react with thiophene by adding to the double bond and undergoing a ring-opening pathway. Subsequently, an additional NO_3 molecule will add to the S−C double bond, then ejecting an SO_2 molecule. An observed secondary formation of SO_2 in the process of thiophene oxidation implies a potential bias in SO_2 concentration estimates based only on primary emissions.

3.1. Constrained Sulfurous Product Distribution by IC Results. As mentioned in Section 2.2, a combination of the measured aerosol volume concentration, effective density, mass fraction of sulfate-related fragments in mAMS, and IC measurements of SO_4^{2-} allowed us to determine the contribution of OS/sulfonate species to the measured sulfate concentrations. NO_2/O_3 experiments yielded an average total sulfate mass concentration of 36.2 ± 2.1 $\mu g/m^3$. Of this total, 34.8 ± 3.4% was determined to be SO_4^{2-}, while the remaining ∼65% was due to OS and/or sulfonate products. This contrasted with the O_3 only control experiments, which yielded a total mass concentration of 20.2 ± 2.2 $\mu g/m^3$ with 49.1 ± 5.9% of it attributed to SO_4^{2-} and 50.9 ± 5.9% to OS/sulfonate products (Figure 4).

The fractions of SO_4^{2-} observed in NO_2/O_3 and ozonolysis conditions showed a significant statistical difference (p = 0.0137) as determined by the Šídák multiple comparison test, which confirmed that the nighttime NO_2/O_3 oxidation condition was not primarily driven by ozonolysis. As discussed above, the Criegee intermediates have been shown to be produced during the ozonolysis of olefins, providing another potential pathway for thiophene oxidation or gas phase reactions between intermediate products. Additionally, ozonolysis can lead to formation of OH radicals,[59,60] which can

https://doi.org/10.1021/acsestair.4c00164
ACS EST Air 2024, 1, 1637−1649

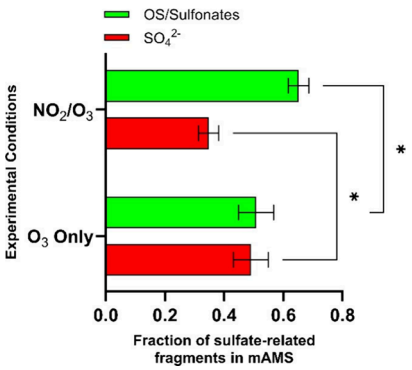

Figure 4. Comparison of SO_4^{2-} and OS/sulfonate fractions in sulfur-containing secondary aerosol fragments observed by mAMS under ozonolysis and NO_2/O_3 experimental conditions. Statistical significance of results with a p value < 0.05 was indicated by *.

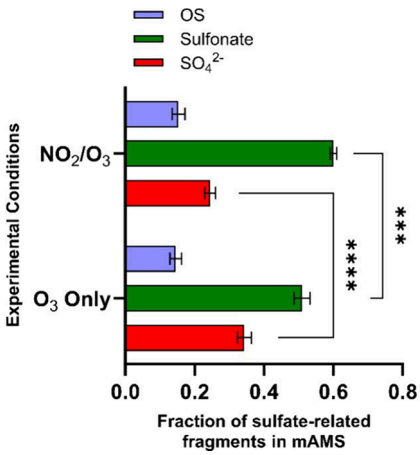

Figure 5. Fractions of SO_4^{2-}, OS, and sulfonate products in total sulfur-containing secondary aerosol fragments observed by mAMS. Statistical significance with a p value < 0.0001 was indicated by ****, while statistical significance with a p value < 0.001 was indicated by ***.

react with SO_2 to form $HOSO_2$, an important step in OH-driven formation of atmospheric H_2SO_4.[61] When considering the impact of these OH radicals as an oxidant in the chamber, IC results showed no SO_4^{2-} production during these experiments. This implied that during our base experiments, the OH radical played a key role in the formation of SO_4^{2-}, and removal of this oxidant may shut down or severely hinder the pathway to SO_4^{2-} formation. OH radicals can also be produced through the reaction of HO_2 and NO_3,[62] ozonolysis of olefin species,[27,59,60] and potentially isomerization reactions of other intermediate species.[63] Since these reactions cannot be ruled out within this study, it is difficult to determine the significance of this OH production pathway relative to OH production from the ozonolysis of olefins due to the inability to constrain HO_2 concentration. The difference in fractions of SO_4^{2-} emphasizes that different oxidation mechanisms dominate each condition. The fractions of SO_4^{2-} and OS/sulfonates were not compared to N_2O_5 conditions due to the technical limitation of synthesizing atmospherically relevant concentrations of NO_3 from N_2O_5 experiments described above.

3.2. mAMS Fragmentation Pattern-Based Fractionation. The relative fractions of each class of sulfur-containing compounds were determined using mAMS sulfur standard fragmentation patterns, as described in Section 2.2 (Figure 5). In NO_2/O_3 experiments, SO_4^{2-} was responsible for 24.5 ± 1.60% of the total sulfate signal, while sulfonates and OS contributed to 60.1 ± 0.94% and 15.4 ± 1.89%, respectively. In contrast, in the ozonolysis control experiments, 34.4 ± 1.94% of the sulfate was associated with SO_4^{2-}, while 51.0 ± 2.31% and 14.6 ± 1.72% were identified as sulfonates and OS, respectively.

Sulfate product contributions calculated through mAMS fragmentation pattern deconvolutions showed a statistical difference for sulfonates (p < 0.001) and SO_4^{2-} (p < 0.0001) under the two atmospheric conditions as determined by the Šídák multiple comparison test; however, there was no statistical difference between the observed OS contributions. Under both conditions, sulfonates dominated the majority of sulfur containing compounds observed, with SO_4^{2-} being the second-largest category. Despite this similarity in trends between product compound classes, mAMS fractionation confirmed that nighttime oxidation of thiophene differed in the extent of SO_4^{2-} production between nighttime chemistry and pure ozonolysis conditions. While formation of SO_4^{2-} was observed under all three conditions, it is clear that ozonolysis favors formation of SO_4^{2-} more than NO_3-driven oxidation conditions due to the higher fraction of SO_4^{2-} observed. However, the exact reason for this cannot be determined and should be investigated in future mechanistic studies. The large fraction of sulfonates observed in Figure 5 compared to OS and SO_4^{2-} fractions has potential mechanistic implications for initiation of thiophene oxidation. Direct attack of NO_3 on the sulfur atom of thiophene prior to ring opening would be the most efficient mechanism for forming sulfonate products, though future studies are needed to determine the mechanism and first-generational products that lead to sulfonate compounds, OS compounds, and SO_4^{2-}. It is also possible that the ring opening pathway of oxidation may be able to produce sulfonate products. However, a more in-depth mechanistic study is required to determine more definitive pathways of oxidation, as no mechanism for this formation is known at this time.

This method of constraining sulfurous product distributions is relatively new, with very few studies testing its accuracy and precision compared to the more traditional offline analytical methods, such as IC. Here, we compare the inorganic sulfate, SO_4^{2-}, fraction of total sulfate in NO_2/O_3 and ozonolysis experiments determined by both methods. As shown in Figure 6, there was a statistical difference determined by the Šídák multiple comparisons test between the SO_4^{2-} fraction estimated by either method in the NO_2/O_3 condition (p = 0.0023). Similarly, a statistical difference was observed between the results obtained from mAMS fragmentations vs IC in the ozonolysis condition (p = 0.0171). Despite this disjoint in percentage of total sulfate observed by either method, both methods suggest a higher fraction of SO_4^{2-} in ozonolysis conditions compared to NO_2/O_3. The difference in estimated fractions will be discussed further in Section 3.4.

3.3. Particulate Organosulfur Product Identification. Major sulfur-containing product identities investigated through the LC/QQQ-MS precursor ion scan revealed the sulfonate and OS candidates fragment into bisulfite ion (HSO_3^- at m/z 81), sulfite ion radical ($SO_3^{-\bullet}$ at m/z 80), bisulfate ion (HSO_4^- at m/z 97), and sulfate ion radical ($SO_4^{-\bullet}$ at m/z 96), respectively.[47] These nominal precursor masses were then

https://doi.org/10.1021/acsestair.4c00164
ACS EST Air 2024, 1, 1637−1649

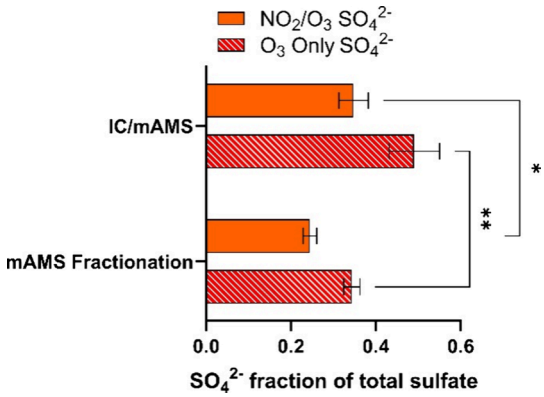

Figure 6. IC calculated mass fractions of SO_4^{2-} for both NO_2/O_3 and ozonolysis conditions compared to the SO_4^{2-} fractions deduced from the mAMS fragmentation patterns. A p value of $p < 0.05$ was indicated by *, while a p value of $p < 0.01$ was indicated by **.

compared to the LC/Q-ToF-MS accurate mass data through a target search to determine the formulas of OS/sulfonate compounds in the thiophene-derived aerosols. This study focused on the identification of products resulting from the NO_3 initiated oxidation pathways (i.e., products observed under both NO_2/O_3 and N_2O_5 conditions). Future research is needed to investigate the interplay of NO_3 and O_3 in the nighttime oxidation of thiophene and its multigenerational product formation—specifically, the role of O_3 in modulating later-generation product formation.

Each peak in the total ion chromatograph was extracted to search for precursors of m/z 80, 81, 96, and 97. OS compounds can fragment into all four species, while sulfonate compounds fragment into only $SO_3^{-\bullet}$ and HSO_3^-. For example, m/z 153 was identified as a precursor to fragment into m/z 97 and m/z 81, as shown in Figure 7A,B.

Observations of m/z 153 under both 97 and 81 precursor ion scans suggested a sulfate structure. After obtaining the exact mass through LC/Q-ToF-MS, the same parameters were kept, and the sample was analyzed by tandem MS scanning for m/z 152.9872. The collision-induced dissociation (CID) of identified precursors in tandem MS analysis revealed that sulfates and sulfonates could be distinguished by their fragmentation patterns, as sulfonates cannot fragment into m/z 96, whereas OS compounds will exhibit fragmentation patterns with a high intensity at m/z 96 and low to medium intensity at m/z 80 and 81. The resulting spectrum, shown in Figure 7C above, was used to confirm the presence of $SO_4^{-\bullet}$ and $SO_3^{-\bullet}$ peaks, indicating the presence of an OS compound at this exact mass.

Nominal masses observed using precursor ion scans produced a targeted list of compounds to identify exact masses of using LC/Q-ToF MS. A total of 29 exact masses and empirical formulas were identified using LC/Q-ToF MS. The 12 highest abundance signals were selected for tandem MS analysis including 6 compounds hypothesized to be OS and 6 compounds hypothesized to be sulfonates as suggested by precursor ion scan results. Compounds that fragment into m/z 96 or 97 were determined to be OS compounds, while compounds that only fragmented into m/z 80 or 81 were determined to be sulfonate compounds. All products recorded by LC/Q-ToF MS are shown in Table S6, however, compounds not selected for tandem MS analysis will not be discussed. The identified sulfur-containing products were

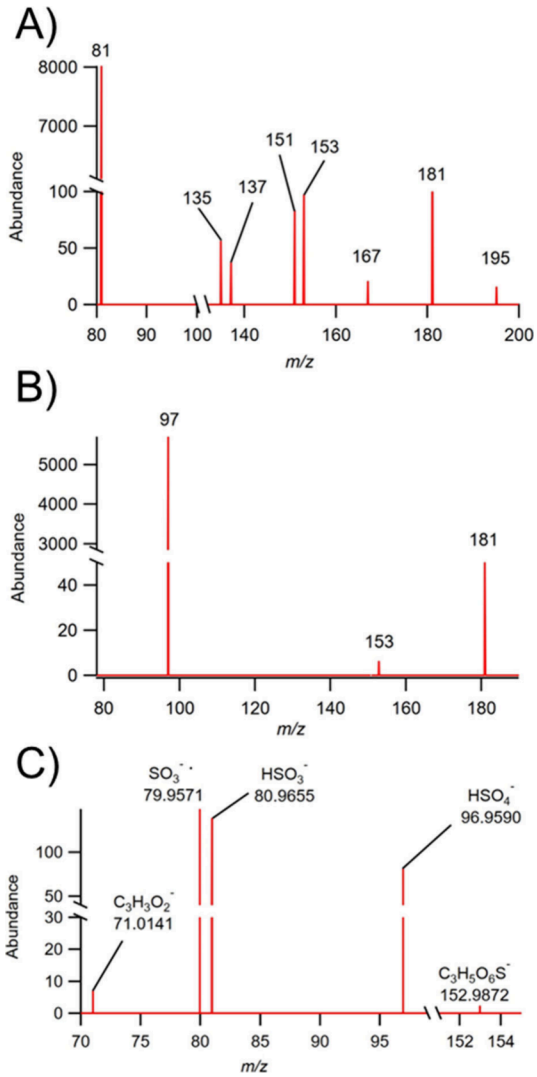

Figure 7. (A) Precursor ion scan of NO_2/O_3 particle extract with retention time of 9.250−10.307 min for the 81-precursor spectrum and (B) retention time of 1.150−2.425 min for the 97-precursor spectrum showing a precursor for fragments 81 and 97 at nominal m/z 153, indicating fragmentation of an OS compound. (C) Tandem MS spectrum at a retention time of 1.096−3.291 scanning for m/z 152.9872. Fragments shown show a peak for HSO_3^- and HSO_4^-, indicating the presence of a sulfate functional group.

displayed in Figure 8 and color-coded according to their sulfur functional group, as confirmed by LC/QQQ-MS, LC/Q-ToF-MS, and the subsequent tandem MS experiments. A full list of the exact masses, molecular formulas, observed tandem MS fragments, and sulfur species types is provided in Table S5, including several peaks that share the same nominal mass that are difficult to distinguish in graphical representation in Figure 8. Products ranged in carbon number from 1 to 6; however, the majority fell at or below a 4-carbon chain backbone. The appearance of compounds with a carbon count greater than 4 implies potential gas phase reactions between smaller carbon-count alkoxy radicals (RO) or alkyl peroxy radicals (RO_2). Although condensed phase reactions may be possible, it is likely that these reactions will take place in the gas phase due to the lower molecular weight and oxygen number of intermediate products. This would then be followed by partitioning of the higher carbon and oxygen count

https://doi.org/10.1021/acsestair.4c00164
ACS EST Air 2024, 1, 1637−1649

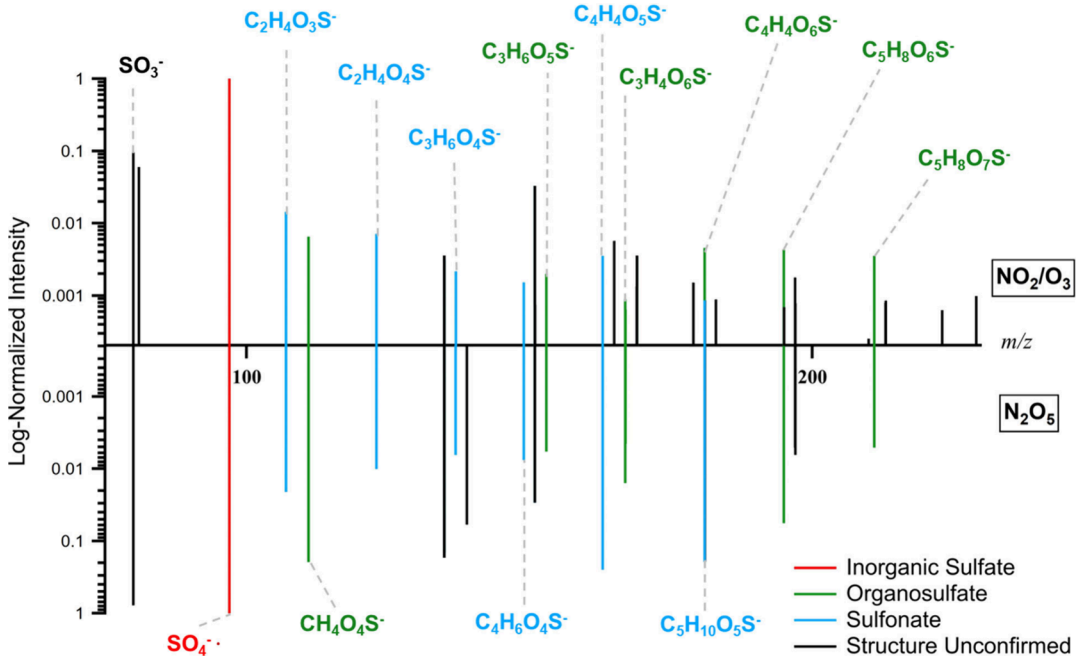

Figure 8. Sulfur-containing secondary aerosol products identified by LC/MS-based methods under the NO_2/O_3 condition displayed against the N_2O_5 control experiment. Labeled peaks were observed in both conditions and color- coded according to sulfur-containing product type as identified by tandem MS. Intensity was normalized to the highest peak, SO_4^{2-}, and displayed in log scale.

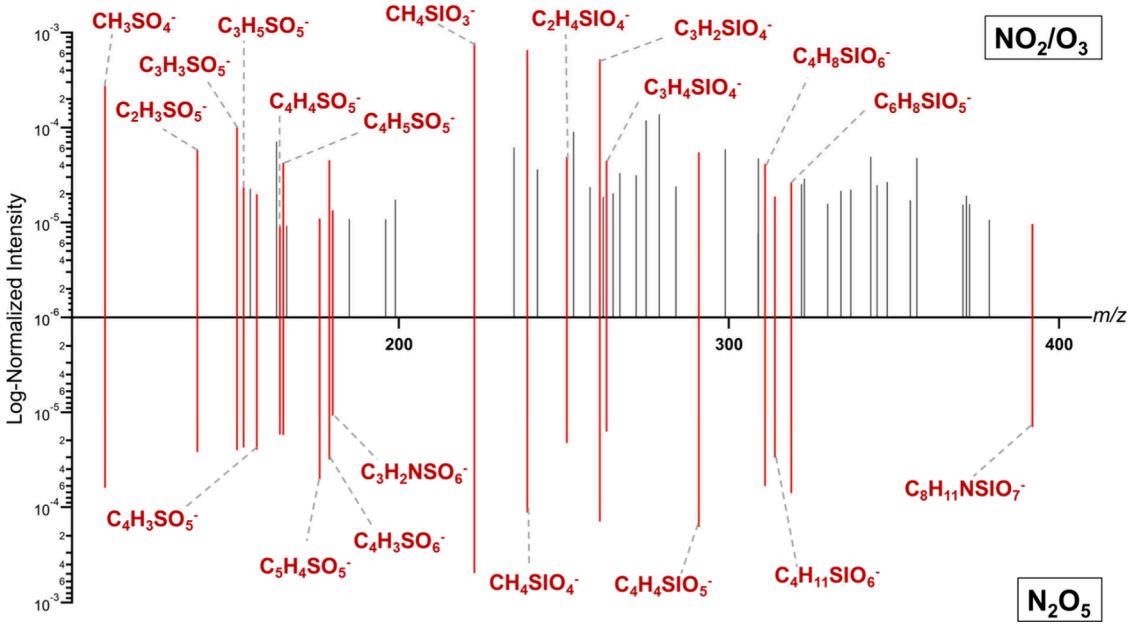

Figure 9. Summary of CIMS observed sulfur-containing organic products categorized according to carbon chain length. Intensity was normalized to the I^- + $(H_2O)I^-$ signals and displayed in log scale. Products displayed in red were observed and identified under both NO_2/O_3 and N_2O_5 conditions, providing evidence that these compounds resulted from the NO_3 initiated oxidation pathway.

products to the condensed phase. We identified more sulfonate compounds (in number) than OS compounds, in line with the results of the mAMS fragmentation pattern differences shown in Figure 5. For all compounds confirmed as either a sulfonate or OS in the current study, their precursor ion scan data and tandem MS spectra similar to those presented in Figure 7 are available in SI (Figures S4−S14).

A wide variety of sulfur-containing aerosol products was observed by FIGAERO ToF-CIMS, resulting in a more thorough profile of sulfur-containing products than could be constrained by any single MS method. The instrument was tuned using methanesulfonic acid (MSA), and signal response was tested using MSA and methyl sulfate standards (Figures S16 and S17). All observed sulfur-containing products are displayed in Figure 9. Fitting results for observed compounds are shown in Table S7 for NO_2/O_3 conditions and Table S8 for N_2O_5 conditions. Sulfur-containing compounds that were confirmed to have resulted from NO_3 oxidation (i.e., compounds present in both conditions) were identified and highlighted in red to emphasize their abundance and

https://doi.org/10.1021/acsestair.4c00164
ACS EST Air 2024, 1, 1637−1649

distribution. The formation of detected products of a carbon count higher than 4 is likely the result of gas phase isomerization reactions or dimerization reactions between thiophene and other subsequent generational products. Further oxidation to subsequent ring opening would likely be a competition between O_3, OH, and NO_3.

There was an overlap of 9 compounds observed by both the LC/MS and CIMS methods. Of the products unique to FIGAERO-ToF-CIMS analysis, we observed two notable compounds containing nitrogen. Due to the susceptibility of nitrate and nitro groups to hydrolysis, compounds such as $C_3H_2NSO_6$ and $C_8H_{11}NSO_7$ could not be observed through LC/MS. Consistent with these observations from LC/MS, the largest proportion of OS/sulfonate products observed by CIMS were C4 compounds, with the second largest being a tie between C3 and C5 compounds. Many of the sulfur-containing products shared similar temperatures of volatilization, with max signal observed ∼140 °C. Thermograms of two detected compounds are shown in Figure S18.

3.4. Potential Limitations. First, the conditions selected in this experiment are a potential limitation of this study, as the ratios of products may change drastically depending on various oxidant concentrations. Since NO_2 and O_3 concentrations are extremely high near the biomass burning emission source and quickly decrease during photochemical O_3 production and NO_2 oxidation, it is likely that the high amounts of oxidants near the source may change the observed OS and sulfonates along with each class of compound's relative concentration.

The current mAMS analysis assumes that all the sulfur-containing compounds have similar relative ionization efficiency (RIE) values. In the mAMS-based method of sulfate family fractionation, since we consider ratios of several fragment ions from each sulfate family, the effect of differences in RIEs cancels out. However, we still rely on mAMS-based quantification of total sulfate when calculating IC-based organosulfur fractions, which is sensitive to RIEs of each sulfate family. Given the lower RIE of OS or sulfonate species relative to SO_4^{2-},[46] we expect that the absolute concentration of total sulfates in mAMS is being underestimated, which leads to underestimating the OS/sulfonate fractions from the IC. Data in Figures 4 and 5 are consistent with this. In Figure 5, the sum of OS and sulfonate species contributes to 75% of the S-containing species for NO_2/O_3 conditions as predicted by the mAMS fragmentation method. On the other hand, the IC-based calculations shown in Figure 4 predicted a total OS and sulfonate fraction of ∼65% for the same conditions.

This study strived to constrain the fate of sulfur into three sulfur-containing categories, while identifying the OS and sulfonate products resulting from NO_3 oxidation. However, due to the high concentration of thiophene used for particle concentration needed for offline analysis, there is likely competition between OH radicals, O_3, NO_3, and other reactions with RO, RO_2, and Criegee biradicals. Partitioning of secondary oxidation products such as SO_2 to particle phase with subsequent particle phase reactions is also possible, as shown by Fung et al. (2022)[28] for the oxidation of DMS.

Furthermore, during particle generation and filter collection, a small fraction of particles was likely lost to the chamber walls as volume decreased. However, all samples for various offline analysis were collected simultaneously or through identical protocols, so any particle loss experienced would likely be experienced uniformly across all conditions and samples. Last empirical formulas identified through FIGAERO−CIMS are intriguing; however, since this method does not have tandem MS functionality, future studies are required for confirmation and structural elucidation.

3.5. Atmospheric Implications. The wide variety of OS and sulfonate compounds empirically identified here emphasizes the importance of nighttime oxidation of understudied reduced organosulfur VOCs as an underrepresented source of SO_4^{2-}, OS, and sulfonate in the atmosphere. During the oxidation process, significant amounts of sulfonates, OS, and SO_4^{2-} are formed, all of which are well-known to have environmental impacts. Sulfur oxidation products have a strong impact on climate and chemical processes. OS and sulfonates are well-known to cause changes in droplet surface tension by disrupting the hydrogen bonding intermolecular forces between water molecules, thereby reducing surface tension and reducing the potential to act as cloud condensation nuclei.[64]

OS/sulfonates with a carbon chain of only one or two may provide more hydrogen bonding sites due to the highly oxygenated SO_4 or SO_3 groups, and as such, they are only weakly surface active due to the smaller hydrophobic portion of the molecule.[64] In contrast, longer carbon chain OS/sulfonate compounds have a more prominent impact on the critical supersaturation required to activate as a cloud condensation nuclei as well as the growth and evaporation rates of droplets.[65,66] With the wide variety of carbon chain lengths produced in the oxidation of the thiophene model system, the high concentrations within smoke plumes will have complex impacts on the short-term climate and particle phase chemical and physical properties in the impacted area. These products are currently unaccounted for in group contribution models predicting aerosol properties. The non-negligible contribution of OS/sulfonate compounds produced from reduced organosulfur oxidation shows that prediction of CCN formation, albedo, radiative forcing, and particle acidity within and downwind of wildfire burn areas cannot be estimated through consideration of SO_4^{2-} alone, and further development of models is needed to accurately predict the impacts of organosulfur VOC oxidation on these particle physical and chemical properties.[64,66−69]

Similarly, SO_4^{2-} concentrations are directly linked to the pH of aerosol particles or cloud droplets. The effects of pH on droplet and particle chemical pathways are still being explored; however, it is understood that pH plays a large role in what reactions may be feasible in the atmosphere and during aqueous processing. The fractions of SO_4^{2-} observed through this study can be applied to thiophene emission factors of various flora species to estimate the impact of individual biomass burning events on the regional atmospheric sulfate budget.

Specifically, results of this study in conjunction with findings from Jiang et al. (2019)[40] and Hatch et al. (2015)[6] make it possible to predict thiophene contribution to the secondary SO_4^{2-} budget within biomass burning plumes. Assuming all of thiophene is consumed and following eq 5, where EF_{thio} is the emission factor of thiophene, Y_{SA} represents the SA yield of thiophene, f_{SO_4} represents the sulfate fraction observed by mAMS, and f_{inorg} is the fraction of total sulfate attributed to SO_4^{2-}, the formation rate of SO_4^{2-} was calculated for Ponderosa Pine, which is a common species throughout North America and is often present in both prescribed and wildfire burn areas.[70]

https://doi.org/10.1021/acsestair.4c00164
ACS EST Air 2024, 1, 1637−1649

$$EF_{thio} \times Y_{SA} \times f_{SO_4} \times f_{inorg} = \frac{\mu g\ SO_4}{kg\ fuel\ burned} \quad (5)$$

Using EF_{thio} of 4.6×10^{-3} g thiophene/kg biomass burned,[6] Y_{SOA} of 0.35,[40] f_{SO_4} of 0.266, and f_{inorg} of 0.303, we determine 1.30×10^{-4} g SO_4^{2-} are formed for every kg of Ponderosa Pine burned during wildfire events. While the formation of SO_4^{2-} through the oxidation of thiophene is low, large-scale burning events may consume fuel quantities large enough to impact aerosol sulfate content. Furthermore, additional work should be carried out to constrain how thiophene and other reduced organosulfur oxidation products affect the physical and chemical properties of atmospheric aerosols, such as surface tension, cloud formation, and particle acidity, compared to products of other analogous heterocyclic aromatic VOC systems.

■ ASSOCIATED CONTENT

Supporting Information

The Supporting Information is available free of charge at https://pubs.acs.org/doi/10.1021/acsestair.4c00164.

Preparation of oxidants in chamber experiments (Text S1); MS instrumentation parameters used for LC/QQQ-MS precursor ion scan and LC/Q-ToF-MS high resolution MS data acquisition (Text S2); Filter collection procedure for offline analysis (Text S3); Sonication Effect on OS Standards (Text S4); A complete list of experiments for thiophene oxidation under three experimental conditions (Table S1); Sulfur standard fragmentation patterns observed by mAMS (Table S2); Fragment ion ratios used for linear combination coefficients determined from averages of all compounds of each class (Table S3); Observed experimental mAMS fractionation signals and ratios used to constrain SO_4^{2-}, OS, and sulfonate products through linear combination (Table S4); Molecular compositions of major sulfur-containing products in thiophene-derived secondary aerosols (Table S5); LC/Q-ToF MS observed sulfur-containing aerosol products for NO_2/O_3 conditions (Table S6); Accurate mass fitting results for FIGAERO-ToF CIMS data from NO_2/O_3 experiments (Table S7); Accurate mass fitting results for FIGAERO-ToF CIMS data from N_2O_5 experiments (Table S8); Extracted ion chromatogram and mass spectra for sulfate standard comparing vortex and sonication extraction effects (Figure S1); Time profiles of N_2O_5 concentrations during the experiments under NO_2/O_3 conditions compared to N_2O_5 only controls (Figure S2); Simulated NO_3 concentration under $[NO_2]/[O_3]$ = 0.1 experimental conditions plotted against N_2O_5 and O_3 measurements (Figure S3); Time series of NO_2, O_3, and particle volume concentrations during O_3 only and N_2O_5 experiments (Figure S4); Precursor ion scan and tandem MS spectra for identified OS and sulfonate compounds. (Figures S5−S15); Time series of gas phase signals for methanesulfonic acid during the instrumental tuning process (Figure S16); Time series of the gas phase signal for methyl sulfate during the instrumental tuning process (Figure S17); Example thermograms of detected oxygenated sulfur products (Figure S18) (PDF)

■ AUTHOR INFORMATION

Corresponding Authors

Roya Bahreini − *Department of Environmental Sciences, University of California, Riverside, California 92521, United States;* orcid.org/0000-0001-8292-5338; Phone: +1-951-827-4506; Email: roya.bahreini@ucr.edu

Ying-Hsuan Lin − *Department of Environmental Sciences, University of California, Riverside, California 92521, United States;* orcid.org/0000-0001-8904-1287; Phone: +1-951-827-3785; Email: ying-hsuan.lin@ucr.edu

Authors

Michael Lum − *Department of Environmental Sciences, University of California, Riverside, California 92521, United States;* orcid.org/0000-0001-5829-5452

Kunpeng Chen − *Department of Environmental Sciences, University of California, Riverside, California 92521, United States;* orcid.org/0000-0002-9430-9257

Bradley Ries − *Department of Environmental Sciences, University of California, Riverside, California 92521, United States*

Linhui Tian − *Department of Environmental Sciences, University of California, Riverside, California 92521, United States;* orcid.org/0009-0009-2147-1518

Raphael Mayorga − *Department of Chemistry, University of California, Riverside, California 92521, United States*

Yumeng Cui − *Department of Environmental Sciences, University of California, Riverside, California 92521, United States*

Nilofar Raeofy − *Department of Environmental Sciences, University of California, Riverside, California 92521, United States*

David Cocker − *Department of Chemical and Environmental Engineering, University of California, Riverside, California 92521, United States;* orcid.org/0000-0002-0586-0769

Haofei Zhang − *Department of Chemistry, University of California, Riverside, California 92521, United States;* orcid.org/0000-0002-7936-4493

Complete contact information is available at: https://pubs.acs.org/10.1021/acsestair.4c00164

Notes

The authors declare no competing financial interest.

■ ACKNOWLEDGMENTS

This work was supported by NSF AGS-1953905 and the UCR Hellman Fellowship granted to Ying-Hsuan Lin. Michael Lum was supported by a NSF graduate research fellowship. We thank David Lyons of the UCR ESRL for his assistance with IC operation, as well as Dr. Jie Zhou of the UCR Analytical Chemistry Instrumentation Facility (ACIF) for his assistance with LC/Q-ToF-MS (acquired by NSF CHE-1828782) operation.

■ REFERENCES

(1) Tiedemann, A. R. Combustion losses of sulfur from forest foliage and litter. *For. Sci.* **1987**, *33* (1), 216−223.

(2) Akagi, S. K.; Yokelson, R. J.; Wiedinmyer, C.; Alvarado, M. J.; Reid, J. S.; Karl, T.; Crounse, J. D.; Wennberg, P. O. Emission factors for open and domestic biomass burning for use in atmospheric models. *Atmos. Chem. Phys.* **2011**, *11* (9), 4039−4072.

(3) Friedli, H. R.; Atlas, E.; Stroud, V. R.; Giovanni, L.; Campos, T.; Radke, L. F. Volatile organic trace gases emitted from North American wildfires. *Global Biogeochem. Cycles* **2001**, *15* (2), 435−452.
(4) Meinardi, S.; Simpson, I. J.; Blake, N. J.; Blake, D. R.; Rowland, F. S. Dimethyl disulfide (DMDS) and dimethyl sulfide (DMS) emissions from biomass burning in Australia. *Geophys. Res. Lett.* **2003**, *30* (9), 1454.
(5) Simpson, I. J.; Akagi, S. K.; Barletta, B.; Blake, N. J.; Choi, Y.; Diskin, G. S.; Fried, A.; Fuelberg, H. E.; Meinardi, S.; Rowland, F. S.; et al. Boreal forest fire emissions in fresh Canadian smoke plumes: C1-C10 volatile organic compounds (VOCs), CO_2, CO, NO_2, NO, HCN and CH_3CN. *Atmos. Chem. Phys.* **2011**, *11* (13), 6445−6463.
(6) Hatch, L. E.; Luo, W.; Pankow, J. F.; Yokelson, R. J.; Stockwell, C. E.; Barsanti, K. C. Identification and quantification of gaseous organic compounds emitted from biomass burning using two-dimensional gas chromatography−time-of-flight mass spectrometry. *Atmos. Chem. Phys.* **2015**, *15* (4), 1865−1899.
(7) Yokelson, R. J.; Saharjo, B. H.; Stockwell, C. E.; Putra, E. I.; Jayarathne, T.; Akbar, A.; Albar, I.; Blake, D. R.; Graham, L. L. B.; Kurniawan, A.; et al. Tropical peat fire emissions: 2019 field measurements in Sumatra and Borneo and synthesis with previous studies. *Atmos. Chem. Phys.* **2022**, *22* (15), 10173−10194.
(8) Sharifi, M. S.; Douroudgari, H.; Vahedpour, M. Chemical insights into the atmospheric oxidation of thiophene by hydroperoxyl radical. *Sci. Rep.* **2021**, *11* (1), 13049.
(9) Rao, G.; Vejerano, E. P. Partitioning of volatile organic compounds to aerosols: a review. *Chemosphere* **2018**, *212*, 282−296.
(10) Kroll, J. H.; Ng, N. L.; Murphy, S. M.; Varutbangkul, V.; Flagan, R. C.; Seinfeld, J. H. Chamber studies of secondary organic aerosol growth by reactive uptake of simple carbonyl compounds. *J. Geophys. Res. Atmos.* **2005**, *110*, No. D23207.
(11) Van Buren, J.; Cuthbertson, A. A.; Ocasio, D.; Sedlak, D. L. Ubiquitous production of organosulfates during treatment of organic contaminants with sulfate radicals. *Environ. Sci. Technol. Lett.* **2021**, *8* (7), 574−580.
(12) Glasius, M.; Thomsen, D.; Wang, K.; Iversen, L. S.; Duan, J.; Huang, R.-J. Chemical characteristics and sources of organosulfates, organosulfonates, and carboxylic acids in aerosols in urban Xi'an, Northwest China. *Sci. Total Environ.* **2022**, *810*, No. 151187.
(13) Atkinson, R.; Carter, W. P. L. Kinetics and mechanisms of the gas-phase reactions of ozone with organic compounds under atmospheric conditions. *Chem. Rev.* **1984**, *84* (5), 437−470.
(14) Atkinson, R.; Aschmann, S. M.; Carter, W. P. L. Kinetics of the reactions of O_3 and OH radicals with furan and thiophene at 298 ± 2 K. *Int. J. Chem. Kinet.* **1983**, *15* (1), 51−61.
(15) Shiroudi, A.; Deleuze, M. S. Theoretical study of the oxidation mechanisms of thiophene initiated by hydroxyl radicals. *J. Mol. Model.* **2015**, *21* (11), 301.
(16) Macleod, H.; Jourdain, J. L.; Le Bras, G. Absolute rate constant for the reaction of OH with thiophene between 293 and 473 K. *Chem. Phys. Lett.* **1983**, *98* (4), 381−385.
(17) Wine, P. H.; Thompson, R. J. Kinetics of OH reactions with furan, thiophene, and tetrahydrothiophene. *Int. J. Chem. Kinet.* **1984**, *16* (7), 867−878.
(18) Martin, D.; Jourdain, J. L.; LeBras, G. Kinetic study for the reactions of OH radicals with dimethylsulfide, diethylsulfide, tetrahydrothiophene, and thiophene. *Int. J. Chem. Kinet.* **1985**, *17* (12), 1247−1261.
(19) Wallington, T. J. Kinetics of the gas phase reaction of OH radicals with pyrrole and thiophene. *Int. J. Chem. Kinet.* **1986**, *18* (4), 487−496.
(20) Lee, J. H.; Tang, I. N. Absolute rate constants for the hydroxyl radical reactions with ethane, furan, and thiophene at room temperature. *J. Chem. Phys.* **1982**, *77* (9), 4459−4463.
(21) Kaduk, B. A.; Toby, S. The reaction of ozone with thiophene in the gas phase. *Int. J. Chem. Kinet.* **1977**, *9* (5), 829−840.
(22) Cabañas, B.; Martín, P.; Salgado, S.; Baeza, M. T.; López, M. R.; Martínez, E. A kinetic study of gas-phase reaction of thiophene with NO_3 by using absolute and relative methods. *Chem. Phys. Lett.* **2002**, *358* (5), 401−406.
(23) Cabañas, B.; Baeza, M. T.; Martín, P.; Salgado, S.; Villanueva, F.; Monedero, E.; Wirtz, K. Products and mechanism of the NO_3 reaction with thiophene. *J. Atmos. Chem.* **2005**, *51* (3), 317−335.
(24) Cabañas, B.; Baeza, M. T.; Martín, P.; Salgado, S.; Villanueva, F.; Monedero, E.; Díaz De Mera, Y. Reaction of the NO_3 radical with some thiophenes: Kinetic study and a correlation between rate constant and EHOMO. *Int. J. Chem. Kinet.* **2006**, *38* (9), 570−576.
(25) Zhang, W.; Wang, T.; Feng, C.; Du, B.; Mu, L. Computational studies on the mechanisms for the gas-phase reaction between thiophene and NO_3. *Chem. Phys. Lett.* **2008**, *467* (1), 52−57.
(26) Atkinson, R.; Aschmann, S. M.; Winer, A. M.; Carter, W. P. L. Rate constants for the gas-phase reactions of nitrate radicals with furan, thiophene, and pyrrole at 295 ± 1 K and atmospheric pressure. *Environ. Sci. Technol.* **1985**, *19* (1), 87−90.
(27) Wayne, R. P. *Chemistry of Atmospheres*; Oxford University Press, 2000.
(28) Fung, K. M.; Heald, C. L.; Kroll, J. H.; Wang, S.; Jo, D. S.; Gettelman, A.; Lu, Z.; Liu, X.; Zaveri, R. A.; Apel, E. C.; et al. Exploring dimethyl sulfide (DMS) oxidation and implications for global aerosol radiative forcing. *Atmos. Chem. Phys.* **2022**, *22* (2), 1549−1573.
(29) Sarwar, G.; Kang, D.; Henderson, B. H.; Hogrefe, C.; Appel, W.; Mathur, R. Examining the impact of dimethyl sulfide emissions on atmospheric sulfate over the continental U.S. *Atmosphere* **2023**, *14* (4), 660.
(30) Liu, T.; Chan, A. W. H.; Abbatt, J. P. D. Multiphase oxidation of sulfur dioxide in aerosol particles: implications for sulfate formation in polluted environments. *Environ. Sci. Technol.* **2021**, *55* (8), 4227−4242.
(31) Bruggemann, M.; Xu, R.; Tilgner, A.; Kwong, K. C.; Mutzel, A.; Poon, H. Y.; Otto, T.; Schaefer, T.; Poulain, L.; Chan, M. N.; et al. Organosulfates in ambient aerosol: state of knowledge and future research directions on formation, abundance, fate, and importance. *Environ. Sci. Technol.* **2020**, *54* (7), 3767−3782.
(32) Blair, S. L.; Macmillan, A. C.; Drozd, G. T.; Goldstein, A. H.; Chu, R. K.; Paša-Tolić, L.; Shaw, J. B.; Tolić, N.; Lin, P.; Laskin, J.; et al. Molecular characterization of organosulfur compounds in biodiesel and diesel fuel secondary organic aerosol. *Environ. Sci. Technol.* **2017**, *51* (1), 119−127.
(33) Koss, A. R.; Sekimoto, K.; Gilman, J. B.; Selimovic, V.; Coggon, M. M.; Zarzana, K. J.; Yuan, B.; Lerner, B. M.; Brown, S. S.; Jimenez, J. L.; et al. Non-methane organic gas emissions from biomass burning: identification, quantification, and emission factors from PTR-ToF during the FIREX 2016 laboratory experiment. *Atmos. Chem. Phys.* **2018**, *18* (5), 3299−3319.
(34) Semmens, E. O.; Leary, C. S.; West, M. R.; Noonan, C. W.; Navarro, K. M.; Domitrovich, J. W. Carbon monoxide exposures in wildland firefighters in the United States and targets for exposure reduction. *J. Expo. Sci. Environ. Epidemiol.* **2021**, *31* (5), 923−929.
(35) Decker, Z. C. J.; Robinson, M. A.; Barsanti, K. C.; Bourgeois, I.; Coggon, M. M.; Digangi, J. P.; Diskin, G. S.; Flocke, F. M.; Franchin, A.; Fredrickson, C. D.; et al. Nighttime and daytime dark oxidation chemistry in wildfire plumes: an observation and model analysis of FIREX-AQ aircraft data. *Atmos. Chem. Phys.* **2021**, *21* (21), 16293−16317.
(36) Mayorga, R.; Chen, K.; Raeofy, N.; Woods, M.; Lum, M.; Zhao, Z.; Zhang, W.; Bahreini, R.; Lin, Y.-H.; Zhang, H. Chemical structure regulates the formation of secondary organic aerosol and brown carbon in nitrate radical oxidation of pyrroles and methylpyrroles. *Environ. Sci. Technol.* **2022**, *56* (12), 7761−7770.
(37) Chen, K.; Raeofy, N.; Lum, M.; Mayorga, R.; Woods, M.; Bahreini, R.; Zhang, H.; Lin, Y.-H. Solvent effects on chemical composition and optical properties of extracted secondary brown carbon constituents. *Aerosol Sci. Technol.* **2022**, *56* (10), 917−930.
(38) Chen, K.; Mayorga, R.; Hamilton, C.; Bahreini, R.; Zhang, H.; Lin, Y.-H. Contribution of carbonyl chromophores in secondary brown carbon from nighttime oxidation of unsaturated heterocyclic

volatile organic compounds. *Environ. Sci. Technol.* **2023**, *57* (48), 20085−20096.
(39) Chen, K.; Mayorga, R.; Raeofy, N.; Lum, M.; Woods, M.; Bahreini, R.; Zhang, H.; Lin, Y.-H. Effects of nitrate radical levels and pre-existing particles on secondary brown carbon formation from nighttime oxidation of furan. *ACS Earth Space Chem.* **2022**, *6* (11), 2709−2721.
(40) Jiang, H.; Frie, A. L.; Lavi, A.; Chen, J. Y.; Zhang, H.; Bahreini, R.; Lin, Y.-H. Brown carbon formation from nighttime chemistry of unsaturated heterocyclic volatile organic compounds. *Environ. Sci. Technol. Lett.* **2019**, *6* (3), 184−190.
(41) Chen, K.; Hamilton, C.; Ries, B.; Lum, M.; Mayorga, R.; Tian, L.; Bahreini, R.; Zhang, H.; Lin, Y.-H. Relative humidity modulates the physicochemical processing of secondary brown carbon formation from nighttime oxidation of furan and pyrrole. *ACS ES&T Air* **2024**, *1* (5), 426−437.
(42) Singh, H. B.; Anderson, B. E.; Brune, W. H.; Cai, C.; Cohen, R. C.; Crawford, J. H.; Cubison, M. J.; Czech, E. P.; Emmons, L.; Fuelberg, H. E.; et al. Pollution influences on atmospheric composition and chemistry at high northern latitudes: Boreal and California forest fire emissions. *Atmos. Environ.* **2010**, *44* (36), 4553−4564.
(43) Bell, D. M.; Pospisilova, V.; Lopez-Hilfiker, F.; Bertrand, A.; Xiao, M.; Zhou, X.; Huang, W.; Wang, D. S.; Lee, C. P.; Dommen, J.; et al. Effect of OH scavengers on the chemical composition of α-pinene secondary organic aerosol. *Environ. sci. Atmos.* **2023**, *3* (1), 115−123.
(44) Bahreini, R.; Keywood, M. D.; Ng, N. L.; Varutbangkul, V.; Gao, S.; Flagan, R. C.; Seinfeld, J. H.; Worsnop, D. R.; Jimenez, J. L. Measurements of secondary organic aerosol from oxidation of cycloalkenes, terpenes, and m-xylene using an aerodyne aerosol mass spectrometer. *Environ. Sci. Technol.* **2005**, *39* (15), 5674−5688.
(45) Decarlo, P. F.; Slowik, J. G.; Worsnop, D. R.; Davidovits, P.; Jimenez, J. L. Particle morphology and density characterization by combined mobility and aerodynamic diameter measurements. Part 1: Theory. *Aerosol Sci. Technol.* **2004**, *38* (12), 1185−1205.
(46) Chen, Y.; Xu, L.; Humphry, T.; Hettiyadura, A. P. S.; Ovadnevaite, J.; Huang, S.; Poulain, L.; Schroder, J. C.; Campuzano-Jost, P.; Jimenez, J. L.; et al. Response of the Aerodyne aerosol mass spectrometer to inorganic sulfates and organosulfur compounds: applications in field and laboratory measurements. *Environ. Sci. Technol.* **2019**, *53* (9), 5176−5186.
(47) Hettiyadura, A. P. S.; Al-Naiema, I. M.; Hughes, D. D.; Fang, T.; Stone, E. A. Organosulfates in Atlanta, Georgia: anthropogenic influences on biogenic secondary organic aerosol formation. *Atmos. Chem. Phys.* **2019**, *19* (5), 3191−3206.
(48) Dickerson, R. R.; Anderson, D. C.; Ren, X. On the use of data from commercial NO_x analyzers for air pollution studies. *Atmos. Environ.* **2019**, *214*, No. 116873.
(49) Cui, Y.; Frie, A. L.; Dingle, J. H.; Zimmerman, S.; Frausto-Vicencio, I.; Hopkins, F.; Bahreini, R. Influence of ammonia and relative humidity on the formation and composition of secondary brown carbon from oxidation of 1-methylnaphthalene and longifolene. *ACS Earth Space Chem.* **2021**, *5* (4), 858−869.
(50) Day, D. A.; Campuzano-Jost, P.; Nault, B. A.; Palm, B. B.; Hu, W.; Guo, H.; Wooldridge, P. J.; Cohen, R. C.; Docherty, K. S.; Huffman, J. A.; et al. A systematic re-evaluation of methods for quantification of bulk particle-phase organic nitrates using real-time aerosol mass spectrometry. *Atmos. Meas. Technol.* **2022**, *15* (2), 459−483.
(51) Ng, N. L.; Brown, S. S.; Archibald, A. T.; Atlas, E.; Cohen, R. C.; Crowley, J. N.; Day, D. A.; Donahue, N. M.; Fry, J. L.; Fuchs, H.; et al. Nitrate radicals and biogenic volatile organic compounds: oxidation, mechanisms, and organic aerosol. *Atmos. Chem. Phys.* **2017**, *17* (3), 2103−2162.
(52) Wang, G.; Zhang, F.; Peng, J.; Duan, L.; Ji, Y.; Marrero-Ortiz, W.; Wang, J.; Li, J.; Wu, C.; Cao, C.; et al. Particle acidity and sulfate production during severe haze events in China cannot be reliably inferred by assuming a mixture of inorganic salts. *Atmos. Chem. Phys.* **2018**, *18* (14), 10123−10132.
(53) Green, J. R.; Fiddler, M. N.; Holloway, J. S.; Fibiger, D. L.; McDuffie, E. E.; Campuzano-Jost, P.; Schroder, J. C.; Jimenez, J. L.; Weinheimer, A. J.; Aquino, J.; et al. Rates of wintertime atmospheric SO_2 oxidation based on aircraft observations during clear-sky conditions over the Eastern United States. *J. Geophys. Res. Atmos.* **2019**, *124* (12), 6630−6649.
(54) Mauldin III, R. L.; Berndt, T.; Sipilä, M.; Paasonen, P.; Petäjä, T.; Kim, S.; Kurtén, T.; Stratmann, F.; Kerminen, V. M.; Kulmala, M. A new atmospherically relevant oxidant of sulphur dioxide. *Nat.* **2012**, *488* (7410), 193−196.
(55) Criegee, R.; Wenner, G. Die ozonisierung des 9,10-oktalins. *Justus Liebigs Ann. Chem.* **1949**, *564* (1), 9−15.
(56) Criegee, R. Mechanism of ozonolysis. *Angew. Chem., Int. Ed.* **1975**, *14* (11), 745−752.
(57) Rickly, P. S.; Guo, H.; Campuzano-Jost, P.; Jimenez, J. L.; Wolfe, G. M.; Bennett, R.; Bourgeois, I.; Crounse, J. D.; Dibb, J. E.; DiGangi, J. P.; et al. Emission factors and evolution of SO_2 measured from biomass burning in wildfires and agricultural fires. *Atmos. Chem. Phys.* **2022**, *22* (23), 15603−15620.
(58) Andreae, M. O.; Browell, E. V.; Garstang, M.; Gregory, G. L.; Harriss, R. C.; Hill, G. F.; Jacob, D. J.; Pereira, M. C.; Sachse, G. W.; Setzer, A. W.; et al. Biomass-burning emissions and associated haze layers over Amazonia. *J. Geophys. Res. Atmos.* **1988**, *93* (D2), 1509−1527.
(59) Donahue, N. M.; Kroll, J. H.; Anderson, J. G.; Demerjian, K. L. Direct observation of OH production from the ozonolysis of olefins. *Geophys. Res. Lett.* **1998**, *25* (1), 59−62.
(60) Atkinson, R.; Aschmann, S. M.; Arey, J.; Shorees, B. Formation of OH radicals in the gas phase reactions of O_3 with a series of terpenes. *J. Geophys. Res. Atmos.* **1992**, *97* (D5), 6065−6073.
(61) Yuan, D.-F.; Liu, Y.; Trabelsi, T.; Zhang, Y.-R.; Li, J.; Francisco, J. S.; Guo, H.; Wang, L.-S. Probing the dynamics and bottleneck of the key atmospheric SO_2 oxidation reaction by the hydroxyl radical. *Proc. Natl. Acad. Sci. U.S.A.* **2024**, *121* (6), No. e2314819121.
(62) Emmerson, K. M.; Carslaw, N. Night-time radical chemistry during the TORCH campaign. *Atmos. Environ.* **2009**, *43* (20), 3220−3226.
(63) Berndt, T.; Scholz, W.; Mentler, B.; Fischer, L.; Hoffmann, E. H.; Tilgner, A.; Hyttinen, N.; Prisle, N. L.; Hansel, A.; Herrmann, H. Fast peroxy radical isomerization and OH recycling in the reaction of OH radicals with dimethyl sulfide. *J. Phys. Chem. Lett.* **2019**, *10* (21), 6478−6483.
(64) Bain, A.; Chan, M. N.; Bzdek, B. R. Physical properties of short chain aqueous organosulfate aerosol. *Environ. sci. Atmos.* **2023**, *3* (9), 1365−1373.
(65) Peng, C.; Razafindrambinina, P. N.; Malek, K. A.; Chen, L.; Wang, W.; Huang, R.-J.; Zhang, Y.; Ding, X.; Ge, M.; Wang, X.; et al. Interactions of organosulfates with water vapor under sub- and supersaturated conditions. *Atmos. Chem. Phys.* **2021**, *21* (9), 7135−7148.
(66) Nozière, B.; Baduel, C.; Jaffrezo, J.-L. The dynamic surface tension of atmospheric aerosol surfactants reveals new aspects of cloud activation. *Nat. Commun.* **2014**, *5* (1), 3335.
(67) Davies, J. F.; Zuend, A.; Wilson, K. R. Technical note: The role of evolving surface tension in the formation of cloud droplets. *Atmos. Chem. Phys.* **2019**, *19* (5), 2933−2946.
(68) Hu, K. S.; Darer, A. I.; Elrod, M. J. Thermodynamics and kinetics of the hydrolysis of atmospherically relevant organonitrates and organosulfates. *Atmos. Chem. Phys.* **2011**, *11* (16), 8307−8320.
(69) Riva, M.; Chen, Y.; Zhang, Y.; Lei, Z.; Olson, N. E.; Boyer, H. C.; Narayan, S.; Yee, L. D.; Green, H. S.; Cui, T.; et al. Increasing isoprene epoxydiol-to-inorganic sulfate aerosol ratio results in extensive conversion of inorganic sulfate to organosulfur forms: implications for aerosol physicochemical properties. *Environ. Sci. Technol.* **2019**, *53* (15), 8682−8694.

(70) Veblen, T. T.; Kitzberger, T.; Donnegan, J. Climatic and human influences on fire regimes in ponderosa pine forests in the Colorado front range. *Ecol. Appl.* **2000**, *10* (4), 1178−1195.

https://doi.org/10.1021/acsestair.4c00164
ACS EST Air 2024, 1, 1637−1649